Working Paper Series

Long-term Effects of Redlining on Environmental Risk Exposure

WP 22-09

Claire Conzelmann
Federal Reserve Bank of Richmond

Arianna Salazar-Miranda
MIT

Toàn Phan
Federal Reserve Bank of Richmond

Jeremy S. Hoffman
Science Museum of Virginia

FEDERAL RESERVE BANK OF RICHMOND®
Richmond ▪ Baltimore ▪ Charlotte

Long-term Effects of Redlining on Environmental Risk Exposure

Claire Conzelmann (Federal Reserve Bank of Richmond)*
Arianna Salazar-Miranda (MIT)
Toàn Phan (Federal Reserve Bank of Richmond)*
Jeremy S. Hoffman (Science Museum of Virginia)

November 17, 2022

Abstract

Climate change exacerbates environmental risks such as intensifying extreme precipitation and heat events. Urban design, in turn, can further amplify these background climate stressors through the well-known urban heat island and rainfall effects, which are largely controlled by the local dominance of impervious land covers, surface roughness, and lack of mature tree canopy. While the extent to which present-day exposures and outcomes related to these climate-exacerbated environmental risks in urban areas can be linked to historical policies has received recent attention (Mujahid et al. 2021; Lane et al. 2022; Swope et al. 2022), causal inference within observed correlative associations has yet to be established. Here, we use a boundary design to estimate the persistent, causal effects of redlining on present-day exposure to climate change-exacerbated environmental risks in six large U.S. cities. Properties in areas assigned a lower-credit grade by the Home Owners' Loan Corporation in the 1930s have 3% higher exposure to flood risk and a 0.07°F higher air temperature today compared to similar properties in higher-graded areas. We show that these differences are driven by lower tree canopy coverage and ground surface perviousness (important measures of environmental capital) in lower-graded areas. Our findings establish, for the first time, that the long-lasting effects of historical urban planning policies can be causally linked to present-day unequal exposures to climate risks.

*The views expressed here are those of the authors and should not be interpreted as those of the Federal Reserve Bank of Richmond or the Federal Reserve System. Contacts: claire.conzelmann@rich.frb.org, ariana@mit.edu, toan.phan@rich.frb.org and jhoffman@smv.org.

1 Significance Statement

Climate change exacerbates heat and precipitation extremes, which are further amplified in urban environments. While studies have argued that redlining – the process of denying neighborhoods access to capital based on a discriminatory grading scheme – can be linked to present-day socioeconomic outcomes, observed patterns of inequitable climate risk through this lens remain correlative in nature. Our method of analysis allows us to infer causality between redlining policies in the 1930s and 1940s and present-day climate-exacerbated flood and heat risk in six U.S. cities. This study contributes a first-of-its-kind application of a boundary design to investigate environmental disparity.

2 Introduction

Decades-old housing policies institutionalized at the federal level have had a lasting effect on American society. A prominent example is the "redlining" housing policy pursued by the Home Owners' Loan Corporation (HOLC) in the 1930s. This practice used maps to demarcate neighborhoods according to their perceived lending risk. Although these maps were supposed to reflect lending risk characteristics such as housing age and prices, the racial composition of neighborhoods also played a prominent role in assigning grades. HOLC maps guided the allocation of credit and mortgage lending, which ultimately affected housing markets and home ownership in redlined neighborhoods (Aaronson et al. 2021b).

Redlining was outlawed in the 1960s due to its discriminatory nature, but its legacy continues to shape present-day income and wealth inequality (Krivo and Kaufman 2004; Ross and Yinger 2002; Turner 2003; Appel and Nickerson 2016; Aaronson et al. 2021a,b). However, evidence documenting whether this policy had long-lasting effects on communities' exposure to environmental and climate risks has remained largely unexplored. Filling this gap is key to reducing environmental and health disparities among communities (Banzhaf et al. 2019a,b).

This paper provides novel evidence of the effects of redlining on present-day exposure to environmental risks. We use digitized HOLC maps and combine them with high-resolution data on key environmental risks, including flooding and heat exposure. We estimate the effects of redlining by exploiting the fact that HOLC maps assigned grades to discrete areas throughout cities, with higher grades reflecting a lower perceived risk of lending. The discrete nature of this policy provides a natural experiment where otherwise similar properties end up on opposite sides of HOLC boundaries, receiving different risk grades. We use a boundary design that compares properties in contiguous HOLC areas with different grades to examine whether those assigned a lower grade in the 1930s have higher exposure to flooding and heat-related risks today.

We find that flood risk and heat exposure significantly increase as the HOLC grade worsens. Properties on the lower-graded side of a HOLC boundary have a flood factor 0.06 points higher than properties on the higher-graded side (about a 3% increase in flood risk relative to the sample mean). We also find that temperatures on lower-graded sides are 0.07°F warmer than on higher-graded ones. These estimates are statistically significant at the 1% level.

We then study the mechanisms driving the higher environmental risks in redlined areas. We document that lower-graded areas have less *environmental capital*—the stock of environmental factors that mediate and determine risk. We proxy for environmental capital using street-level vegetation, tree canopy coverage, and ground surface perviousness. These factors can be improved via public and private investments and have been shown to reduce environmental risk (Li et al., 2012; Davis et al., 2016; Xiao and McPherson, 2002). We find that properties on the lower-graded side of a HOLC boundary have less vegetation, less tree canopy, and lower perviousness than properties on the higher-graded side. We interpret these local differences as reflecting a lack of investments in environmental capital on lower-graded sides of HOLC boundaries.

This paper contributes to two primary literatures. First, we contribute to a growing literature documenting the adverse and persistent effects of historical redlining on contemporary outcomes. This literature shows that HOLC maps became an important mechanism guiding the allocation of credit and mortgage lending, which ultimately affected housing markets and home ownership in redlined neighborhoods. For example, Appel and Nickerson (2016) and Aaronson et al. (2021b) document the adverse long-run effects on housing market outcomes of being assigned a lower grade. Krimmel (2018), Faber (2020), and Aaronson et al. (2021a) show that the practice of redlining contributed to a decline in population density, greater segregation, and lower economic opportunity. Methodologically, we build on the work of Aaronson et al. (2021b) and use a boundary design to identify the causal effects of the maps. Different from previous work, we show that the practice of redlining had a persistent impact on environmental risks and environmental capital.

Second, we contribute to the literature on environmental justice. This literature has provided ample evidence showing that, in the U.S., non-Hispanic minorities are disproportionately exposed to pollution, heat, and other environmental risks (see Banzhaf et al., 2019b, for a complete review). For example, Voelkel et al. (2018), Hsu et al. (2021), and Renteria et al. (2022) document a higher heat exposure among non-Hispanic communities of color. Jbaily et al. (2022) document a higher incidence of air pollution among racial and ethnic minorities and lower-income groups, and Colmer et al. (2020) document that air pollution is persistently concentrated in some areas and neighborhoods. Bakkensen and Ma (2020) document that low-income and minority residents are more likely to move into areas with higher flood risks. Wilson (2020) and Hoffman et al. (2020) documents that, on average, redlined areas are currently exposed to higher temperatures. We complement these studies by providing novel causal evidence on the effects of redlining on neighborhoods' exposure to climate and environmental risks. We also explore the mechanisms leading to these differences and document an important role of neighborhoods' environmental capital in determining their exposure.

3 Data

Home Owners' Loan Corporation Maps. We obtained HOLC map shapefiles from the University of Richmond's Digital Scholarship Lab's *Mapping Inequality* database. The project

digitized historical HOLC maps from 239 cities. The maps indicate the grades assigned to different areas in these cities, with grades ranging from A (lowest lending risk) to D (highest lending risk). Our sample consists of nine cities across the U.S. – Baltimore, Boston, Houston, Miami, Los Angeles, New York City, Sacramento, Seattle, and Tampa – for which we have measures of flood risk.[1] HOLC maps of the nine cities are shown in Figure 4 in the Appendix. The maps show that not all city areas received a grade. In our analysis, we focus on those areas that did and explore the consequences of receiving a lower grade.

Measuring Environmental Risk. We use two measures of environmental risk: a flood risk index and a measure of heat exposure. To measure flood risk, we use the First Street Foundation's *Flood Factor*. This is a novel measure of flood risk that assigns a score from one to 10 to each property in the continental U.S. This measure reflects the risk of flooding in the next 30 years, with a value of 1 denoting the lowest risk and a value of 10 the highest. The flood factor is computed using a model that accounts for four major contributors to flooding: rainfall, river overflow, high tide, and coastal storm surge. The First Street Foundation model also accounts for future environmental changes, including sea level rise, which captures the risk of flooding in the face of a changing climate. The model also incorporates information on elevation, ground surface perviousness, and the prevalence of community flood protection measures (such as dunes, wetlands, and seawalls), which make flood risk vary locally even among neighboring properties.

We measure heat exposure using the Urban Heat Island Maps from the National Integrated Heat Health Information System. These maps were created using vehicular traverses to collect ground-based temperature measurements. These are then used to estimate temperatures for the entire urban area at a ten meter resolution. Rather than measuring ambient air temperature or land surface temperatures, these urban heat island maps measure the ground-level temperature, providing a more accurate measure of people's exposure to heat.

Proxies of Environmental Capital. We use three proxies of environmental capital: tree canopy coverage, street-level vegetation, and ground surface perviousness. We measure tree canopy coverage for 2016 using raster data from the National Land Cover Database. These data are available for 30-meter by 30-meter cells and provides the percentage of the cell area that is covered by tree canopy. These estimates are derived from multi-spectral Landsat imagery.

To measure street-level vegetation, we use the *green view index* from the Treepedia database, produced by the MIT Senseable City Lab. The green view index measures the percentage of vegetation in images from Google Street View panoramas. The index is available for points along the street network sampled every 20 meters. This measure complements the tree canopy measure constructed using satellite imagery by providing additional information on the presence of vegetation at the street level.

[1] Our sample also contains measures of heat exposure for six of these cities (Baltimore, Boston, Houston, Los Angeles, Miami, and Seattle).

Finally, we also obtained a measure of ground surface imperviousness for 2016 from the National Land Cover Database, available for 30-meter cells. The database provides the share of developed land that uses impervious surfaces. For ease of interpretation, we define perviousness as 1 minus the imperviousness share.

Summary Statistics. Table 1 presents summary statistics for our measures of environmental risk and capital for the nine cities in our sample and by HOLC grade. The table shows that as one moves from higher-graded to lower-graded cells, there is a sizable decline in our proxies of environmental capital. For example, tree canopy coverage declines from 21.5% to 3.5% and perviousness decreases from 62.7% to 27.7% as we move from A-graded to D-graded areas.

For environmental risks (flooding and heat exposure), there is no systematic pattern across grades. However, mean differences in environmental risk across grades are hard to interpret, since they also capture differences in geographic attributes that vary across locations, such as elevation or coastal proximity. For example, A-graded properties could have a greater flood risk because they are in high-income neighborhoods near the coasts. To separate the role of redlining from other geographic differences, we implement a boundary design. This design compares similar properties on opposite sides of HOLC boundaries, which offer a better comparison group.

Defining the Boundary Sample

To implement our boundary design, we select HOLC boundaries separating areas with different grades and decompose each boundary into straight segments, or borders. Our boundary sample includes properties or cells within a 100-meter buffer of these borders. When constructing the boundary sample, we compute distances as follows. For the flood factor data, we computed the distance from the centroid of each property to the nearest HOLC border. For the tree canopy, ground surface perviousness, and temperature data, we computed the distance from each cell centroid to the nearest HOLC border. Finally for the green view index data, we compute the distance from each sample point to the nearest HOLC border.

Figure 1 describes our sample construction. Panel (a) shows the HOLC map of Baltimore and identifies the borders between polygons of differing grades and their corresponding 100 meter buffers. Panel (b) shows an enlarged map of a selection of the HOLC polygons in Baltimore. The thicker lines represent the HOLC border separating differently graded polygons. The thinner lines show the 100 meter buffer zones around each border. The black and grey points denote the set of properties within the 100 meter buffers. The black points are properties on the higher-graded side of the nearest HOLC border; the grey points are properties on the lower-graded side of the nearest HOLC border.

Our boundary design estimates the effect of a lower HOLC grade by comparing properties on opposite sides of the same border (i.e., the properties lying on opposite sides of the border identified with black or grey dots in Figure 1). The key assumption behind this approach is that properties on different graded sides of the HOLC borders share similar *location fundamentals*—

Table 1: Summary statistics.

	Samples					
	Full Sample	**A grade**	**B grade**	**C grade**	**D grade**	**100m-Boundary Sample**
Environmental risk						
Flood Factor (1 to 10)	1.802 (1.825)	2.026 (2.307)	1.756 (1.852)	1.793 (1.765)	1.805 (1.772)	1.771 (1.748)
Number of properties in flood factor sample	2,409,530	145,888	528,674	1,159,894	575,074	317,029
Temperature (°F)	86.464 (7.235)	86.26 (8.036)	87.255 (7.018)	86.350 (7.166)	85.775 (7.205)	85.85 (6.998)
Number of 10m cells in temperature sample	9,849,451	871,227	2,559,612	4,468,268	1,950,344	1,343,274
Environmental capital						
Green View Index (%)	19.365 (11.542)	29.264 (11.480)	23.326 (11.970)	17.423 (10.279)	17.134 (11.044)	20.634 (11.622)
Number of points in GVI sample	321,131	25,014	60,101	141,732	94,284	45,105
Tree Canopy (%)	8.843 (16.663)	21.505 (22.977)	13.401 (19.423)	6.240 (13.566)	3.486 (10.378)	9.875 (16.818)
Number of 30m cells in tree canopy sample	2,419,037	251,831	552,688	1,066,956	547,195	308,314
Perviousness (%)	37.326 (25.681)	62.686 (24.433)	45.936 (25.573)	31.792 (22.003)	27.745 (22.657)	36.035 (24.367)
Number of 30m cells in perviousness sample	2,419,045	251,830	552,685	1,067,038	547,133	308,341

Note.— The table provides the mean and standard deviation (in parentheses) for the measures of environmental risk and the proxies for environmental capital. The columns break down these statistics by sample, including HOLC areas in our nine cities, A-graded areas, B-graded areas, C-graded areas, and D-graded areas, respectively. The final column reports these statistics for the 100m-boundary sample described in Section 3.

exogenous geographic attributes that may impact climate-related outcomes and differ only in their historical grades.

To verify this assumption, we examine how properties differ in terms of precipitation, soil quality, and elevation on both sides of the HOLC borders. For precipitation, we use data on annual precipitation from the USDA available for 800 meter grids and measured in inches of precipitation per year. For soil quality, we use data on soil water storage available for 10m cells. This is an indicator of soil's ability to retain water, measured in centimeters and ranging from 0 (least) to 150 (highest). For elevation, we use data from the U.S. Geographical Services, which provides raster data on elevation in meters above the sea level available for 1/3 arcsecond cells (approximately 10m cells).

Table 2 reports the average precipitation, soil quality, and elevation on the higher- and lower-graded sides of the HOLC borders in our sample. The last column reports the difference between these means and its standard error. Differences in precipitation and soil quality across

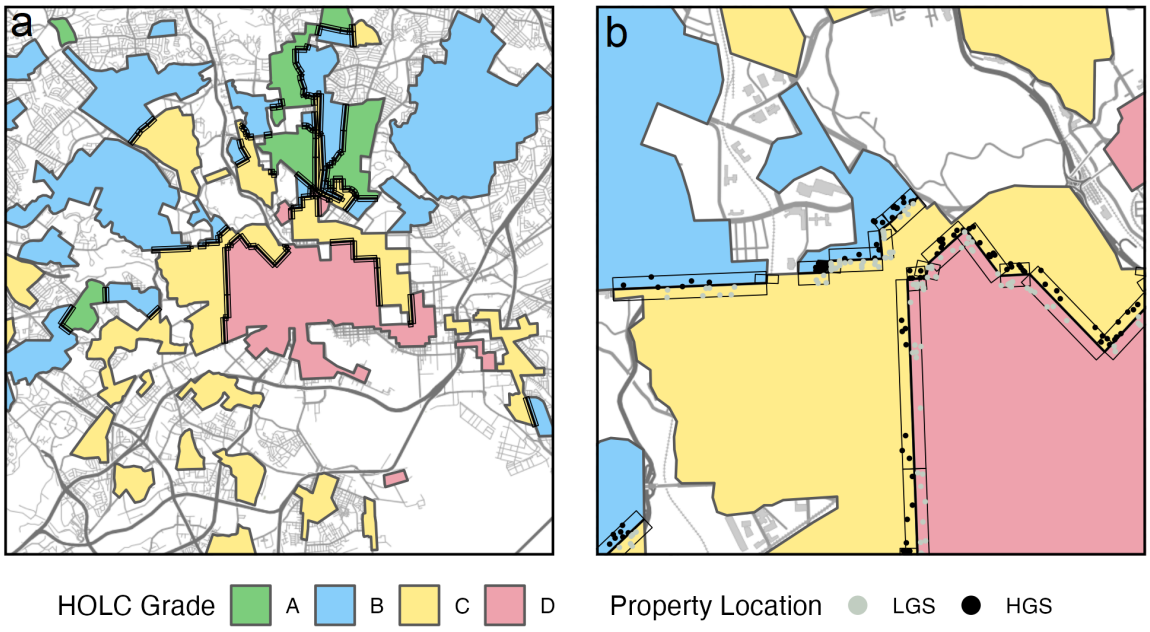

Figure 1: A VISUALIZATION OF SAMPLE CONSTRUCTION. Panel (a) shows the HOLC map of Baltimore with borders and buffer zones between polygons with differing HOLC grades. Panel (b) shows an enlarged map of a sample of the HOLC borders in Baltimore. The thicker lines represent the HOLC border separating differently graded polygons. The thinner lines are 100 meter buffer zones around each border. Only properties (or cells) within the 100 meter buffer zones are included in the sample. A subsample of properties included in the sample are shown on the map; the black properties are on the higher-graded side of the HOLC border, and the grey properties are on the lower-graded side of the HOLC border.

HOLC borders are small and not statistically significant. On the other hand, higher-graded sides have a 3.17-meter higher elevation than lower-graded sides. As a consequence, in our regressions, we will need to control for elevation to account for these differences across HOLC borders.

A second potential concern with our boundary design is that the sample might not be representative of all areas that received a HOLC grade. The last column in Table 1 provides summary statistics for the 100-meter boundary sample and shows that its average environmental risks and capital are comparable to the full sample reported in column 1. This suggests that our estimates for the boundary sample are likely to be representative of the broader impacts of redlining.

Table 2: Location fundamentals for higher and lower-graded sides.

	100m-Boundary Sample		
	Higher-Graded Side	Lower-Graded Side	Difference
Precipitation	35.89421	35.16501	0.729206
			(1.781018)
Number of 800m cells in precipitation sample cells	164	154	
Soil quality	13.60556	13.6027	-0.00285
			(0.008211)
Number of 10m cells in soil quality sample	1,324,287	1,315,116	
Elevation	48.87415	45.7073	3.16685***
			(0.070258)
Number of 1/3 arcsecond cells in elevation sample	1,097,258	1,052,036	

Note.— The table provides the average of each variable on the higher- and lower-graded sides of HOLC borders and the difference in means. Standard errors are in parentheses. The 100m-boundary sample includes observations within 100 meters of a HOLC border in areas with different HOLC grades. Precipitation measures annual rainfall per year in inches. Soil quality measures the amount of available water storage in the soil in centimeters. Elevation measures elevation above sea level in meters. $***p < 0.01, **p < 0.05, *p < 0.1$.

4 The Causal Effects of Redlining on Environmental Risk

To uncover the causal effects of redlining on environmental risk, we estimate the following regression using the 100-meter boundary sample:

$$\text{Environmental Risk}_i = \alpha + \beta_B B_i + \beta_C C_i + \beta_D D_i + \gamma \log \text{elevation}_i + f_b + \epsilon_i. \quad (1)$$

We use flooding and heat exposure as our measures of environmental risk. For flooding, i denotes a property, and we estimate equation (1) at the property level. For heat exposure, i denotes a 10-meter cell, and we estimate equation (1) at the cell level.

The regression explains environmental risk as a function of HOLC grades, treating a grade of A as the excluded category. This is captured by the dummy variables B_i, C_i, and D_i, which indicate the HOLC grade of the area that contains each cell or property. In this model, β_B, β_C, and β_D capture the causal effect of being assigned a grade lower than A. In addition, we control for the log of elevation (which is particularly important for the flood risk), and for border fixed effects f_b, where b is the closest HOLC border to property i. Border fixed effects capture common geographic attributes of the properties and cells near a boundary but on differently graded sides. They ensure that we identify the causal effect of lower HOLC grades by comparing each property or cell to those on the opposite side of the same border. To account for spatial correlation, we cluster errors at the border level.

The left panel of Figure 2 plots the point estimates along with the 95% confidence intervals for $\hat{\beta}_B, \hat{\beta}_C, \hat{\beta}_D$ from equation (1). The figure shows that the flood risk and temperature of cells increases monotonically as the HOLC grade worsens. Properties in B-graded areas have a flood factor that is 0.04 points higher than properties in A-graded areas. This effect more

than triples for properties in D-graded areas, which have a flood factor that is 0.14 points higher than A-graded properties. These estimates are economically significant, amounting to about 2.5% and 8% of the sample standard deviation for the flood risk. Similarly, we see that heat exposure increases as HOLC grade worsens. Compared to cells in A-graded polygons, C-graded cells are approximately 0.11°F hotter, and D-graded cells are 0.15°F hotter. Appendix Table 3 summarizes these results and provides additional information for these regressions.

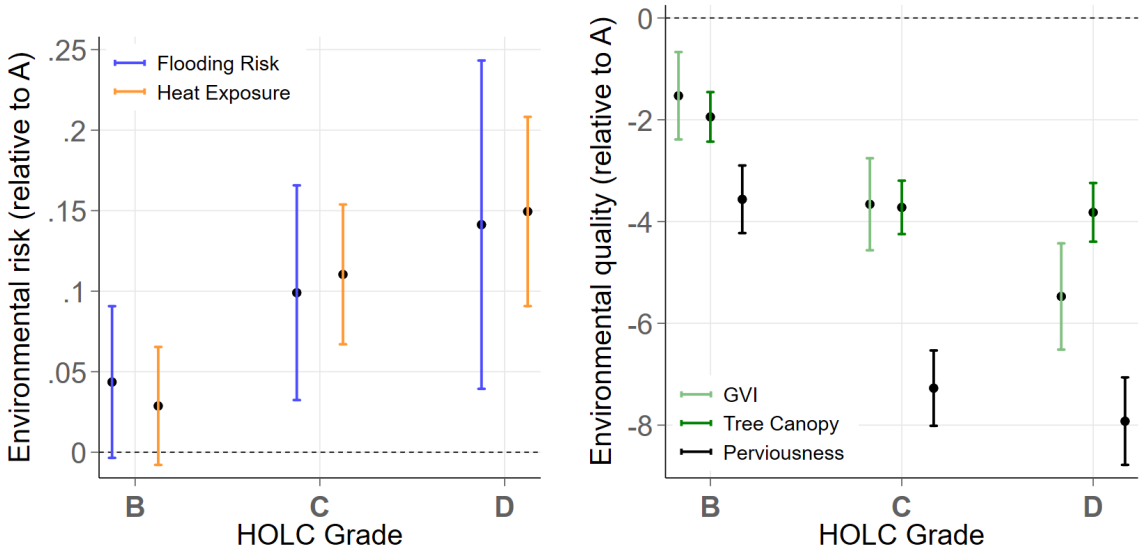

Figure 2: Effects of historical HOLC grades on current environmental risk and capital. The figure plots the point estimates $\hat{\beta}_B, \hat{\beta}_C$, and $\hat{\beta}_D$ (with 95% confidence intervals, standard errors clustered at the border level) from regressing $Y_i = \alpha + \beta_B B_i + \beta_C C_i + \beta_D D_i + \gamma \log \text{elevation}_i + f_b + \epsilon_i$ for our two measures of environmental risk, flood risk and heat exposure (left panel), and our three proxies of environmental capital – green view index (GVI), tree canopy, and perviousness (right panel).

To summarize our results in a parsimonious way, we pool the estimates of equation (1) in a single value capturing the effect of being assigned to a lower-graded area. In particular, we use the boundary sample to estimate the equation:

$$\text{Environmental Risk}_i = \alpha + \beta LGS_i + \gamma \log \text{elevation}_i + f_b + \epsilon_i. \tag{2}$$

In this specification, LGS_i is an indicator for whether cell or property i is on the lower-graded side of the nearest HOLC border.

The left panel in Figure 3 plots the coefficients for LGS_i in equation (2) using flooding and heat exposure as our measures of environmental risk. Being on the lower-graded side of a HOLC border has a statistically and economically significant impact on a property's flood factor, increasing it by approximately 0.06 points. This corresponds to a 3% increase in risk relative to the baseline flood factor. Being on the lower-graded side of a HOLC border also increases exposure to heat. Cells on the lower-graded side are 0.069°F warmer than cells on the higher-graded side of the border. Appendix Table 4 summarizes these results and provides

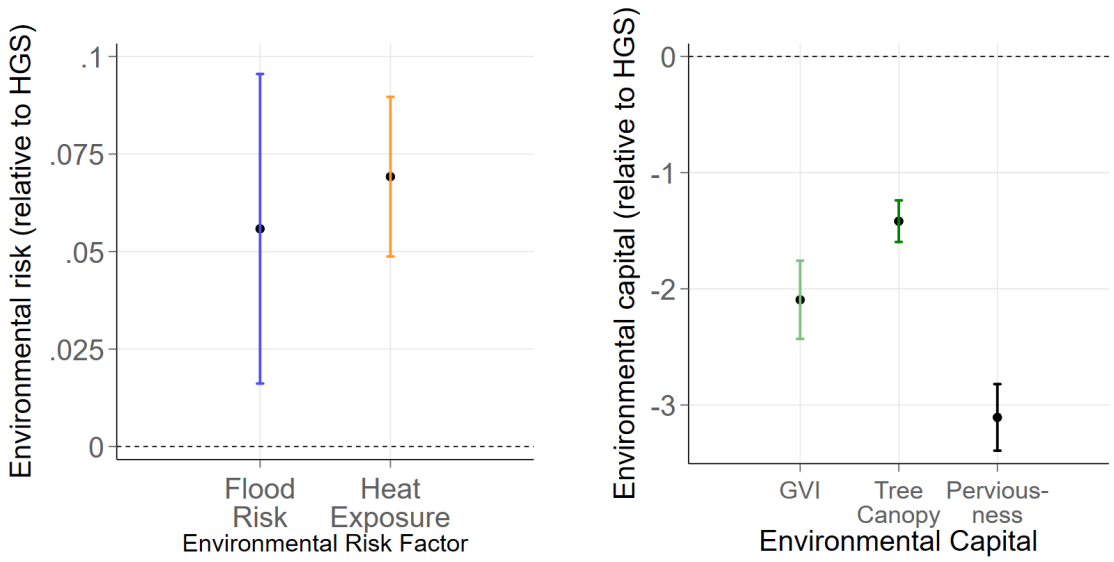

Figure 3: Effects of lower HOLC grade on current environmental risk and capital. The figure plots the point estimate $\hat{\beta}$ (with 95% confidence intervals, standard errors clustered at the border level) from $Y_i = \alpha + \beta LGS_i + \gamma \log \text{elevation}_i + f_b + \epsilon_i$ for our two measures of environmental risk, flood risk and heat exposure (left panel), and our three proxies of environmental capital – green view index (GVI), tree canopy, and perviousness (right panel).

additional information for these regressions. In a city with very high flood risk – such as New Orleans, which has an average flood factor of 8.2 – this 0.06 point increase in flood factor is small, increasing flood risk by around 0.6%. For cities with less frequent and more minor flooding – such as Seattle, which has an average flood factor of 1.6 – this effect on flood factor corresponds to an increase that is more than five times larger (3.5%) than the relative increase for New Orleans.

4.1 The Role of Environmental Capital

We now explore the mechanisms behind the higher environmental risk in lower-graded HOLC areas. We explore the idea that redlining lowers investment in environmental capital, which then manifests into higher environmental risks. A lower HOLC grade can reduce investments in environmental capital for several reasons. For example, lower property values can affect local taxes and the ability of communities to invest in vegetation, trees, and better construction materials (Schwarz et al., 2015; Hope et al., 2006; Kinzig et al., 2005). Further, areas with high income inequality have been linked to lower levels of social capital and community engagement (Alesina and La Ferrara, 2000, 2002; Paarlberg et al., 2018), which could impede a community's investment in public goods. We view our measures of perviousness, tree canopy, and street vegetation as capturing the ability of a community to invest in local public goods that reduce environmental risk. For example, communities could increase their tree coverage and reduce their heat exposure by investing in parks and public gardens. Likewise, communities could

invest in draining systems or in better and more pervious materials to reduce their risk of flooding.

The right panel in Figure 2 reports estimates of equation (1) using our three measures of environmental capital as outcomes. We find that lower HOLC grades lead to reduced perviousness, street vegetation, and tree canopy. Cells in B-graded and D-graded areas have a level of perviousness 3.5 and 7.9 percentage points lower, respectively, than cells in A-graded areas on the opposite site of the HOLC border. These effects are large when compared to an average perviousness of 36.5% in our sample. Likewise, cells in D-graded areas have a tree canopy and green view index 3.8 and 5.5 percentage points lower, respectively, than cells in A-graded areas. These effects are also sizable relative to the sample means in Table 1.

The right panel of Figure 3 reports estimates of equation (2) using our three measures of environmental capital as outcomes. These single measures of the effects of redlining show that being assigned a lower HOLC grade results in a reduction in perviousness of 3.1 percentage points, tree canopy of 1.4 percentage points, and the green view index of 2.1 percentage points. These effects are all sizable at about 5 to 10% of their sample means.

4.2 Robustness Checks

A potential concern with our boundary design sample is that it is not representative of all areas that received a HOLC grade. We provide results from equations (1) and (2) utilizing different samples to corroborate our main findings. Appendix Table 5 offsets our 100-meter boundary sample by 50 meters on either side. The top panel shows that our boundary design is robust to this 50-meter boundary offset. Furthermore, in this sample, each measure of environmental risk increases monotonically as HOLC grade worsens, and each measure of environmental capital decreases monotonically as HOLC grade worsens (bottom panel). Appendix Table 6 presents results from Equations (1) and (2) using properties/cells within 300 meters of each HOLC border with a grade change. When increasing the sample to this distance, we risk the grids becoming less comparable, though most of our results are robust to this sample selection as well.

In another robustness check, we include a specification that controls for the Housing Price Index (HPI) of each property or cell. This is because the difference in housing prices can account for differences in environmental capital that we do not observe. We gather HPI data at the census tract level from the Federal Housing Finance Agency and use the average HPI for each census tract from 2016-2019. Appendix Table 7 shows that our results from equations (1) and (2) are robust to the addition of this control, signaling that the lower environmental capital and higher environmental risk we find in lower-graded properties/cells are not being driven by differences in housing prices. Because lower housing prices are a result of redlining, however, these results should be interpreted with a degree of caution, as the inclusion of the control could introduce selection bias (Angrist and Pischke, 2014).

5 Conclusion

This paper documented the persistent causal impact of the redlining housing policy pursued by the Home Owners' Loan Corporation (HOLC) in the 1930s on present-day exposure to environmental risks. We use a boundary design that compares properties or cells within 100 meters of a HOLC border of differing grades to identify causality. We find that properties on the lower-graded side of a HOLC border have significantly higher flood factor and heat exposure than properties on higher-graded sides. We further find that the higher environmental risks are in part driven by a decline in environmental capital in redlined areas. In particular, we show that properties on the lower-graded side have lower levels of green view index, tree canopy, and ground surface perviousness, which we take to reflect a a lack of investments in public goods that can mitigate environmental risks.

This long-term effect of redlining on environmental risk exposure is relevant for several reasons. First, because higher flood risk typically means the financial risk from flood damage is elevated, increased flood risk could exacerbate the existing economic inequality in these communities. Second, the long-term effects of redlining suggest that policies can significantly impact communities long after their cessation. This highlights the importance not only of ensuring that policies like the HOLC lending practices are not reinstated, but also of creating equitable climate policy that can reduce climate risk exposure in communities experiencing systematic disinvestment and disproportionate exposure to environmental risk due to past discriminatory policies. As sea levels continue to rise, floods continue to increase in frequency, and temperatures keep rising, recognizing the unequal exposure to environmental risks will be crucial to creating place-specific policies that effectively abate future climate risk for all.

References

Aaronson, D., Faber, J., Hartley, D., Mazumder, B., and Sharkey, P. (2021a). The long-run effects of the 1930s HOLC "redlining" maps on place-based measures of economic opportunity and socioeconomic success. *Regional Science and Urban Economics*, 86:103622.

Aaronson, D., Hartley, D., and Mazumder, B. (2021b). The effects of the 1930s HOLC "redlining" maps. *American Economic Journal: Economic Policy*, 13(4):355–92.

Alesina, A. and La Ferrara, E. (2000). Participation in heterogeneous communities. *The Quarterly Journal of Economics*, 115(3):847–904.

Alesina, A. and La Ferrara, E. (2002). Who trusts others? *Journal of Public Economics*, 85(2):207–234.

Angrist, J. D. and Pischke, J.-S. (2014). *The Wages of Schooling*, chapter 6, pages 209–244. Princeton University Press.

Appel, I. and Nickerson, J. (2016). Pockets of poverty: The long-term effects of redlining. *Available at SSRN 2852856*.

Bakkensen, L. A. and Ma, L. (2020). Sorting over flood risk and implications for policy reform. *Journal of Environmental Economics and Management*, 104:102362.

Banzhaf, S., Ma, L., and Timmins, C. (2019a). Environmental justice: Establishing causal relationships. *Annual Review of Resource Economics*, 11:377–398.

Banzhaf, S., Ma, L., and Timmins, C. (2019b). Environmental justice: The economics of race, place, and pollution. *Journal of Economic Perspectives*, 33(1):185–208.

Colmer, J., Hardman, I., Shimshack, J., and Voorheis, J. (2020). Disparities in PM2.5 air pollution in the United States. *Science*, 369(6503):575–578.

Davis, A. Y., Jung, J., Pijanowski, B. C., and Minor, E. S. (2016). Combined vegetation volume and "greenness" affect urban air temperature. *Applied Geography*, 71:106–114.

Faber, J. W. (2020). We built this: Consequences of New Deal era intervention in America's racial geography. *American Sociological Review*, 85(5):739–775.

Hoffman, J. S., Shandas, V., and Pendleton, N. (2020). The effects of historical housing policies on resident exposure to intra-urban heat: A study of 108 US urban areas. *Climate*, 8(1):12.

Hope, D., Gries, C., Casagrande, D., Redman, C. L., Grimm, N. B., and Martin, C. (2006). Drivers of spatial variation in plant diversity across the Central Arizona-Phoenix ecosystem. *Society and Natural Resources*, 19(2):101–116.

Hsu, A., Sheriff, G., Chakraborty, T., and Manya, D. (2021). Disproportionate exposure to urban heat island intensity across major US cities. *Nature Communications*, 12(1):1–11.

Jbaily, A., Zhou, X., Liu, J., Lee, T. H., Kamareddine, L., Verguet, S., and Dominici, F. (2022). Air pollution exposure disparities across US population and income groups. *Nature*, 601(7892):228–233.

Kinzig, A. P., Warren, P., Martin, C., Hope, D., and Katti, M. (2005). The effects of human socioeconomic status and cultural characteristics on urban patterns of biodiversity. *Ecology and Society*, 10(1).

Krimmel, J. (2018). Persistence of prejudice: Estimating the long term effects of redlining. *Working Paper*.

Krivo, L. J. and Kaufman, R. L. (2004). Housing and wealth inequality: Racial-ethnic differences in home equity in the United States. *Demography*, 41(3):585–605.

Lane, H. M., Morello-Frosch, R., Marshall, J. D., and Apte, J. S. (2022). Historical redlining is associated with present-day air pollution disparities in US cities. *Environmental Science & Technology Letters*, 9(4):345–350.

Li, Y.-y., Zhang, H., and Kainz, W. (2012). Monitoring patterns of urban heat islands of the fast-growing Shanghai metropolis, China: Using time-series of Landsat TM/ETM+ data. *International Journal of Applied Earth Observation and Geoinformation*, 19:127–138.

Mujahid, M. S., Gao, X., Tabb, L. P., Morris, C., and Lewis, T. T. (2021). Historical redlining and cardiovascular health: The multi-ethnic study of atherosclerosis. *Proceedings of the National Academy of Sciences*, 118(51):e2110986118.

Paarlberg, L. E., Hoyman, M., and McCall, J. (2018). Heterogeneity, income inequality, and social capital: A new perspective. *Social Science Quarterly*, 99(2):699–710.

Renteria, R., Grineski, S., Collins, T., Flores, A., and Trego, S. (2022). Social disparities in neighborhood heat in the Northeast United States. *Environmental Research*, 203:111805.

Ross, S. L. and Yinger, J. (2002). *The color of credit: Mortgage discrimination, research methodology, and fair-lending enforcement*. MIT press.

Schwarz, K., Fragkias, M., Boone, C. G., Zhou, W., McHale, M., Grove, J. M., O'Neil-Dunne, J., McFadden, J. P., Buckley, G. L., Childers, D., Ogden, L., Pincetl, S., Pataki, D., Whitmer, A., and Cadenasso, M. L. (2015). Trees grow on money: Urban tree canopy cover and environmental justice. *PloS One*, 10(4):e0122051.

Swope, C. B., Hernández, D., and Cushing, L. J. (2022). The Relationship of Historical Redlining with Present-Day Neighborhood Environmental and Health Outcomes: A Scoping Review and Conceptual Model. *Journal of Urban Health*, pages 1–25.

Turner, M. A. (2003). *Discrimination in Metropolitan Housing Markets: Phase 2 – Asians and Pacific Islanders*. DIANE Publishing.

Voelkel, J., Hellman, D., Sakuma, R., and Shandas, V. (2018). Assessing Vulnerability to Urban Heat: A Study of Disproportionate Heat Exposure and Access to Refuge by Socio-Demographic Status in Portland, Oregon. *International Journal of Environmental Research and Public Health*, 15(4).

Wilson, B. (2020). Urban heat management and the legacy of redlining. *Journal of the American Planning Association*, 86(4):443–457.

Xiao, Q. and McPherson, E. G. (2002). Rainfall interception by Santa Monica's municipal urban forest. *Urban Ecosystems*, 6(4):291–302.

A Appendix

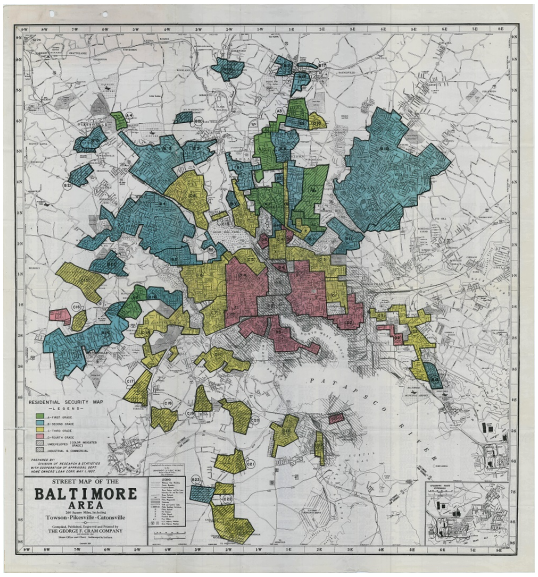

(a) Baltimore

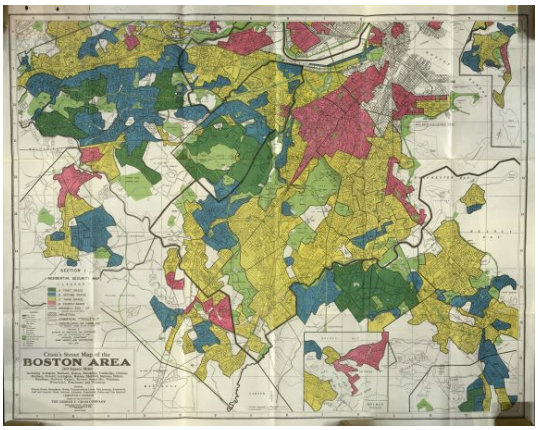

(b) Boston

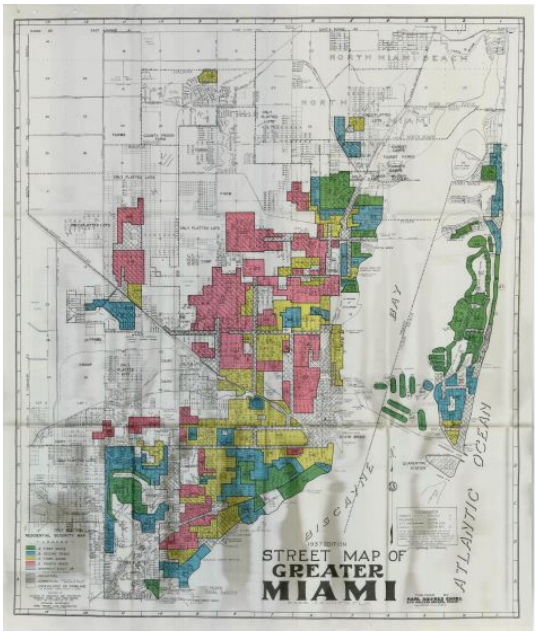

(c) Miami

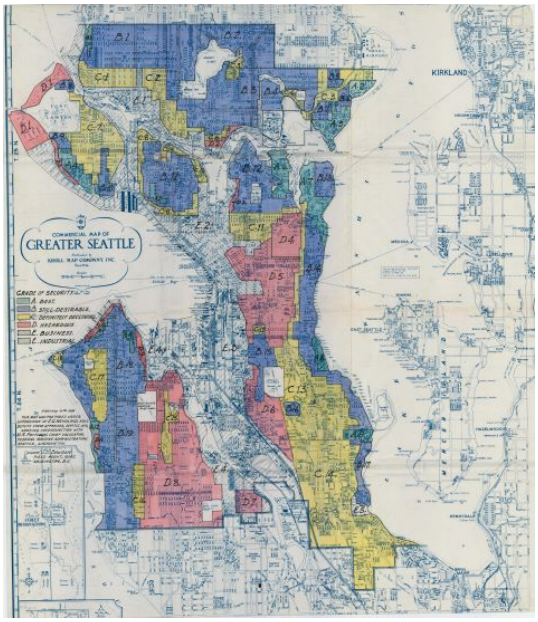

(d) Seattle

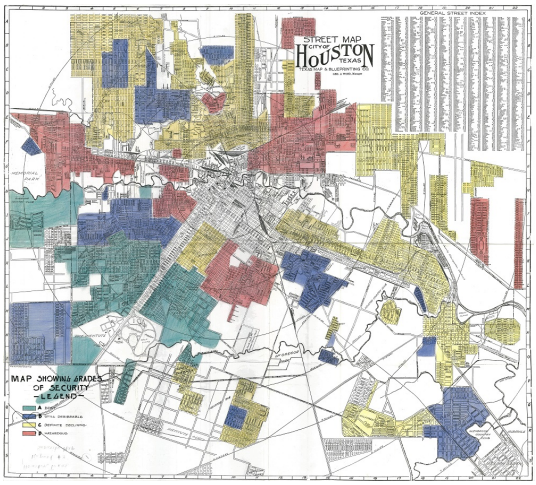

(e) Houston

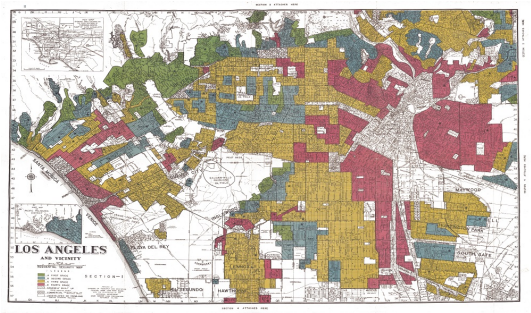

(f) Los Angeles

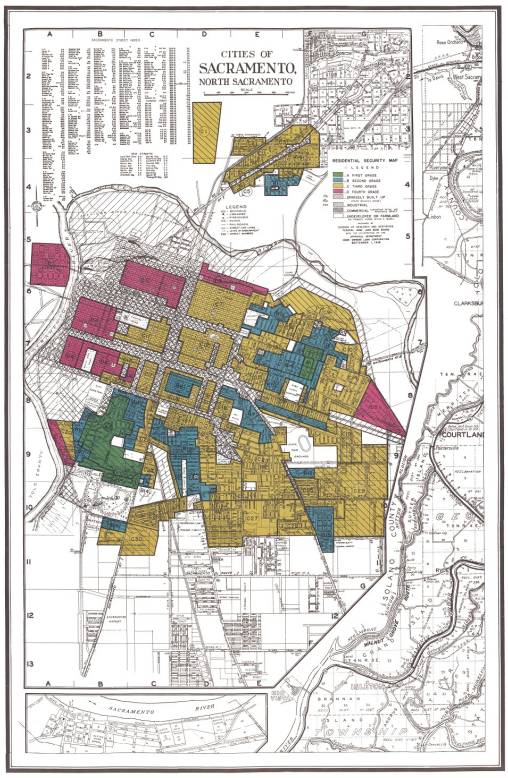

(g) Sacramento

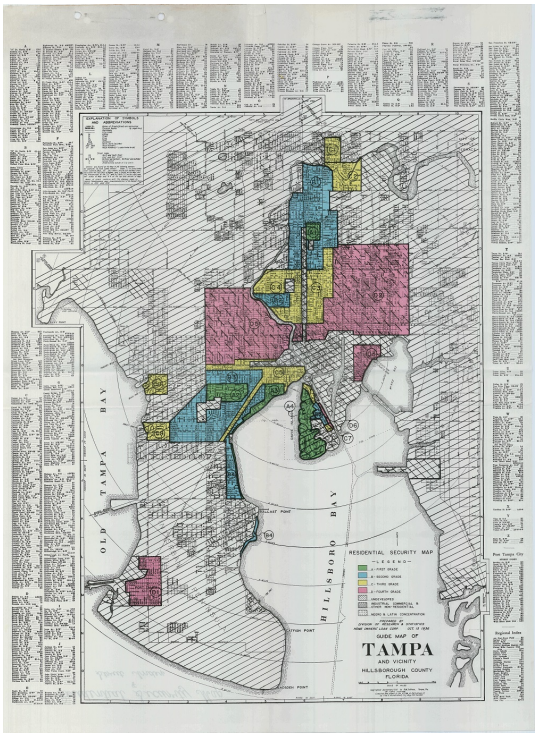

(h) Tampa

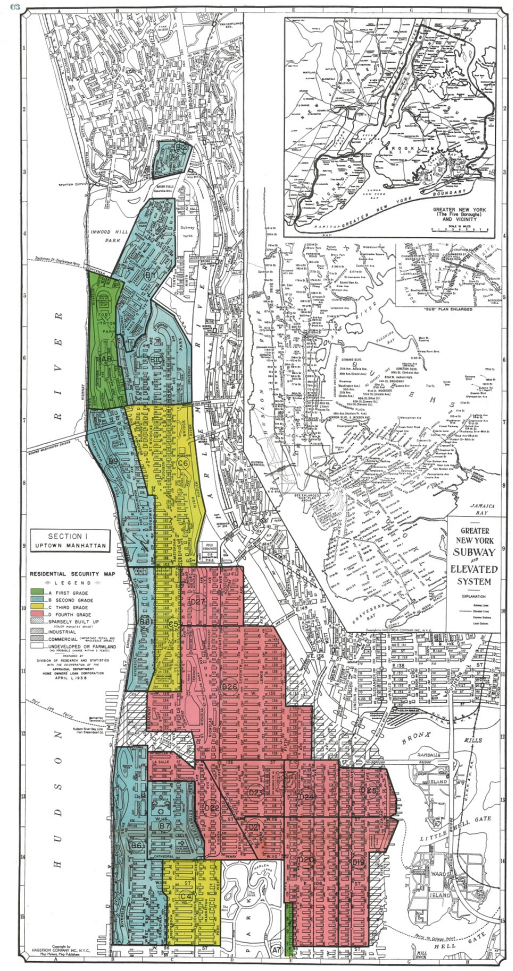

(i) Manhattan

Figure 4: HOLC Map Scans of Cities Included in Sample

Table 3: Effects of Historical HOLC Grade on Current Environmental Risk and Capital

	100m-Boundary Sample				
	Flood Factor	Temperature	GVI	%Canopy	%Perviousness
B Grade	0.044*	0.029	-1.528***	-1.944***	-3.563***
	(0.024)	(0.019)	(0.438)	(0.249)	(0.339)
C Grade	0.099***	0.110***	-3.660***	-3.722***	-7.274***
	(0.034)	(0.022)	(0.461)	(0.268)	(0.378)
D Grade	0.141***	0.149***	-5.472***	-3.819***	-7.923***
	(0.052)	(0.030)	(0.533)	(0.294)	(0.438)
log(elevation)	-1.564***	-0.139***	0.008	0.234***	0.093
	(0.357)	(0.035)	(0.599)	(0.031)	(0.080)
N	316110	1343217	44025	307380	307426
R^2	0.615	0.994	0.659	0.631	0.663

Note.—Flood risk, exposure to heat, GVI, canopy coverage, and perviousness all worsen as HOLC grade worsens. The table shows the results from regressing $Y_i = \alpha + \beta LGS_i + \gamma \log(elev_i) + f_b + \epsilon_i$ using properties and cells i within 100m of nearest HOLC border b, where Y is either Flood Risk, Heat Exposure, Perviousness, Canopy coverage, or Green View Index. Standard errors clustered at border level in parentheses; $***p < 0.01, **p < 0.05, *p < 0.1$.

Table 4: Effects of Lower HOLC Grade on Current Environmental Risk and Capital

	100m-Boundary Sample				
	Flood Factor	Temperature	GVI	%Canopy	%Perviousness
lower-graded Side	0.056***	0.069***	-2.094***	-1.418***	-3.107***
	(0.020)	(0.010)	(0.172)	(0.091)	(0.146)
log(elevation)	-1.564***	-0.139***	0.087	0.229***	0.086
	(0.356)	(0.035)	(0.600)	(0.031)	(0.081)
N	316110	1343217	44025	307380	307426
R^2	0.615	0.994	0.659	0.631	0.662

Note.—Properties/cells on a lower HOLC graded side have worse flood risk, perviousness, canopy coverage, green view indices, and heat risk than those on a higher-graded side. The table shows the results from regressing $Y_i = \alpha + \beta LGS_i + \gamma \log(elev_i) + f_b + \epsilon_i$ using properties and cells i within 100m of nearest HOLC border b, where Y is either Flood Risk, Heat Exposure, Perviousness, Canopy coverage, or Green View Index. Standard errors clustered at border level in parentheses; $***p < 0.01, **p < 0.05, *p < 0.1$.

Table 5: 50M-Boundary Offset

	50m-Boundary Offset Sample				
	Flood Factor	Temperature	GVI	%Canopy	%Perviousness
Lower-Graded Side	0.064***	0.066***	-2.382***	-1.578***	-3.898***
	(0.021)	(0.010)	(0.164)	(0.093)	(0.147)
log(elevation)	-1.382***	-0.153***	-1.076	0.214***	0.128***
	(0.371)	(0.037)	(0.660)	(0.024)	(0.045)
N	300839	1296255	41889	291657	291617
R^2	0.617	0.995	0.664	0.648	0.673
B Grade	0.064**	0.061***	-1.207***	-1.855***	-3.835***
	(0.026)	(0.019)	(0.466)	(0.254)	(0.347)
C Grade	0.116***	0.127***	-3.591***	-3.731***	-8.053***
	(0.035)	(0.022)	(0.478)	(0.271)	(0.383)
D Grade	0.175***	0.154***	-5.842***	-3.971***	-9.699***
	(0.054)	(0.030)	(0.530)	(0.300)	(0.447)
log(elevation)	-1.382***	-0.153***	-1.142*	0.217***	0.130***
	(0.371)	(0.037)	(0.663)	(0.025)	(0.044)
N	300839	1296255	41889	291657	291617
R^2	0.617	0.995	0.664	0.648	0.673

Note.— Table presents results from Equations (1) and (2) using a sample that offsets our 100 meter buffer zones by 50 meters on either side of the HOLC border. The top panel shows results from Equation (2); the bottom panel shows results from Equation (1). Standard errors clustered at border level in parentheses; $***p < 0.01, **p < 0.05, *p < 0.1$.

Table 6: 300M-Boundary Sample

	300M-Boundary Sample				
	Flood Factor	Temperature	GVI	%Canopy	%Perviousness
Lower-Graded Side	0.027	0.106***	-2.184***	-2.016***	-4.165***
	(0.024)	(0.021)	(0.175)	(0.099)	(0.166)
log(elevation)	-1.594***	-0.176***	-0.260	0.303***	0.148
	(0.275)	(0.037)	(0.470)	(0.040)	(0.091)
N	654988	2762811	90404	615672	615735
R^2	0.529	0.992	0.602	0.586	0.611
B Grade	0.040	0.085**	-1.925***	-2.860***	-5.156***
	(0.029)	(0.035)	(0.477)	(0.279)	(0.381)
C Grade	0.084**	0.236***	-4.160***	-5.216***	-10.098***
	(0.042)	(0.040)	(0.506)	(0.296)	(0.426)
D Grade	0.080	0.266***	-5.945***	-5.602***	-11.118***
	(0.061)	(0.057)	(0.569)	(0.318)	(0.486)
log(elevation)	-1.594***	-0.170***	-0.369	0.311***	0.160*
	(0.275)	(0.037)	(0.475)	(0.040)	(0.090)
N	654988	2762811	90404	615672	615735
R^2	0.529	0.992	0.602	0.587	0.612

Note.— Table presents results from Equations (1) and (2) using properties/cells within 300 meters of the nearest HOLC border with a grade change. The top panel shows results from Equation (2); the bottom panel shows results from Equation (1). Standard errors clustered at border level in parentheses; $***p < 0.01, **p < 0.05, *p < 0.1$.

Table 7: Controlling for Housing Price Index

	100m-Boundary Sample				
	Flood Factor	Temperature	GVI	%Canopy	%Perviousness
Lower-Graded Side	0.072***	0.068***	-1.842***	-1.395***	-3.023***
	(0.023)	(0.011)	(0.226)	(0.116)	(0.176)
log(elevation)	-1.215***	-0.119***	-0.304	0.224***	0.084
	(0.357)	(0.037)	(0.780)	(0.031)	(0.084)
HPI	-0.000	-0.000	0.004**	0.003***	0.008***
	(0.000)	(0.000)	(0.002)	(0.001)	(0.001)
N	193768	604595	28007	218251	218322
R^2	0.638	0.970	0.645	0.622	0.622
B Grade	0.032	0.034***	-1.587***	-1.817***	-3.360***
	(0.027)	(0.013)	(0.501)	(0.273)	(0.370)
C Grade	0.107***	0.110***	-3.368***	-3.461***	-6.653***
	(0.038)	(0.018)	(0.568)	(0.304)	(0.422)
D Grade	0.164**	0.143***	-5.162***	-3.407***	-7.222***
	(0.064)	(0.025)	(0.728)	(0.366)	(0.533)
log(elevation)	-1.215***	-0.121***	-0.353	0.228***	0.092
	(0.358)	(0.037)	(0.782)	(0.031)	(0.083)
HPI	-0.000	-0.000	0.004*	0.003***	0.009***
	(0.000)	(0.000)	(0.002)	(0.001)	(0.001)
N	193768	604595	28007	218251	218322
R^2	0.638	0.970	0.645	0.623	0.622

Note.— Table presents results from Equations (1) and (2) with the inclusion of a control for housing price index at the census tract level. The top panel shows results from Equation (2); the bottom panel shows results from Equation (1). Standard errors clustered at border level in parentheses; $***p < 0.01, **p < 0.05, *p < 0.1$.